Three-dimensional charge density wave in the dual heavy fermion system math xmlns="http://www.w3.org/1998/Math/MathML">mrow>mi mathvariant="normal">U/mi>msub>mi>Pt/mi>mn>2/mn>/msub>msub>mi>Si/mi>mn>2/mn>/msub>/mrow>/math>

Valeri Petkov, R. Baumbach, A. M. Milinda Abeykoon, and J. A. Mydosh

Phys. Rev. B **107**, 245101 — Published 1 June 2023

DOI: 10.1103/PhysRevB.107.245101

3D charge density wave in the dual heavy fermion liquid UPt_2Si_2

Valeri Petkov[1], R. Baumbach[2,3], AM. Milinda Abeykoon[4] and J. A. Mydosh[5]

[1]Department of Physics, Central Michigan University, Mt. Pleasant, MI 48858, USA

[2]National High Magnetic Field Laboratory, Florida State University, Tallahassee FL 32310, USA

[3]Department of Physics, Florida State University, Tallahassee, FL 32310, USA

[4]Photon Sciences Division, Brookhaven National Laboratory, Upton, NY 11973, USA

[5]Institute Lorentz, Leiden University, Leiden 2300RA, The Netherlands

Abstract

Heavy ferminon liquids offer via their Kondo lattice diverse possibilities for exotic ground states. Using variable temperature atomic pair distribution function (PDF) analysis, we study the local atomic structure of the "dual" heavy fermion liquid UPt_2Si_2, which exhibits antiferromagnetism consistent with localized 5*f*-electron states and transport properties characteristic to itinerant 5*f*-'*spd*' hybridized electron systems. We show that UPt_2Si_2 exhibits periodic lattice distortions (PLDs) involving both U and Pt atoms that are characteristic to 3D charge density waves. The temperature evolution of the PLDs tracks that of the transport and magnetic properties, suggesting the presence of little-known 5*f*-electron-lattice interactions. We argue that PLDs in heavy fermion liquids in general and in particular in UPt_2Si_2, appear as new degrees of freedom that entangle competing electronic states and, as such, must be accounted for when their rich physics is considered.

1. Introduction

Quantum materials with diverse interactions (lattice, charge, spin and orbital) are at the nexus of efforts to produce novel states of matter. Amongst these materials, strongly correlated *f*-electron systems serve as an especially deep reservoir for novel behaviors, where examples include heavy-fermion Kondo lattices, unconventional superconductors, hidden order, hybridization-gap topological insulators, and Weyl-Kondo semimetals [1-8]. A large number of such systems belong to the $ThCr_2Si_2$ structure-type family, which is derived from the prototypical $BaAl_4$ structure [9-21]. Less well-studied are systems that crystallize in the closely related $CaBe_2Ge_2$-type structure, which, contrary to the $ThCr_2Si_2$ structure, lacks inversion symmetry along the c-axis. Recently, materials with this structure have attracted increased interest because of the discovery of (i) a

possible topological superconductivity in $CeRh_2As_2$ and (ii) a prediction of gapless Weyl-Kondo nodal-lines in $CePt_2Si_2$ and $CeRh_2Ga_2$. [22-29].

This led us to focus on UPt_2Si_2 ($CaBe_2Ge_2$ structure-type), which had long been thought to exhibit prototypical localized *f*-electron behavior with crystal-electric field splitting of the localized U 5*f*-electron states and antiferromagnetic (AF) order at T_N = 34 K [30, 31]. However, several recent studies have challenged this perspective by providing evidence for the presence of 5*f* - conduction'*spd*' electrons hybridization similar to what is seen in other Kondo lattice materials [32-34]. This includes new evidence for coherence behavior in the electrical transport properties; the observation of high magnetic field phase transitions suggesting the presence of Fermi surface instabilities due to a breakdown of the Kondo coherent ground state; inelastic neutron-scattering measurements that are consistent with a dual localized-itinerant 5*f*-electron character; and density functional theory calculations that favor a scenario where the 5*f* electrons of U are mostly itinerant. Furthermore, X-ray-diffraction (XRD) measurements revealed large anisotropic thermal factors for atoms occupying the Si-Pt-Si layers, which were interpreted as an indication of strong crystallographic disorder [35]. This disorder was proposed to be responsible for Anderson localization along the *c* axis of the crystal lattice, resulting in an anisotropic resistivity. However, more recent studies connected this behavior to the emergence of charge density wave (CDW) order at an anomalously large temperatures T_{CDW}= 315 K [29].

Collectively, these behaviors reveal an unusual diversity of phenomena with a potential interplay between Kondo lattice hybridization, CDW and AF orders. However, there remains uncertainty about the inter-relationship between these diverse phenomena and the crystal structure, including the periodic lattice distortions (PLDs) known to accompany CDWs. To clarify these questions, we use variable-temperature atomic pair distribution function (PDF) analysis coupled to structure modeling to study lattice distortions in UPt_2Si_2. We find that UPt_2Si_2 is a rare example of a ternary Fermi liquid where both metallic species are displaced from their position in the undistorted crystal lattice in a correlated manner. The displacements appear above T_{CDW} and evolve nonlinearly with diminishing temperature, increasingly disturbing the spatial coherence of the crystal lattice. Moreover, the deviations from linearity closely track changes in the electronic and magnetic properties, indicating the presence of a little-known strong interaction between lattice, electronic and magnetic degrees of freedom in UPt_2Si_2. Beyond this, our results call for similar local structure studies of other members of $CaBe_2Ge_2$- and $ThCr_2Si_2$-type families of heavy

fermion liquids, where models that neglect lattice distortions and local crystal symmetry breaking may not fully describe the observed fascinating phenomena.

2. Experimental

2.1 *Sample preparation and properties characterization.*

Polycrystalline samples of UPt_2Si_2 were synthesized by arc melting the constituent elements (99.99% pure, lump form) in a 1:2:2 molar ratio of U:Pt:Si. The resulting boule was flipped and re-arced five times to ensure homogeneity. The final product was faceted, indicating the formation of large grains. In-house x-ray diffraction studies on powdered pieces showed that the as-cast UPt_2Si_2 possess a $CaBe_2Ge_2$-type structure (Space Group *P*4/*nmm*), shown in Figure 1(*a*).

Specimens for electrical resistivity measurements were prepared by cleaving fragments from the main boule. This produces slabs of material, to which platinum wires were attached using a micro-spot-welding device. Standard four-wire electrical resistance R(T) measurements were performed for $1.8 < T < 350$ K using a Quantum Design Physical Properties Measurement System (PPMS). Results for the room temperature normalized resistivity R/R_{300K}, shown Figure 1(*b*), are consistent with earlier reports. In particular, R/R_{300K} shows a strongly non-linear evolution with temperature, where clear inflection points are observed at $T_{CDW} = 315$ K and $T_N = 37$ K. Below T_{CDW}, R/R_{300K} increases with decreasing temperatures and goes through a maximum at $T_{coh} = 150$ K. Such a phenomenon is typically observed with Kondo-lattice systems and associated with the formation of coherent hybridization between the *f*- and conduction electron states, leading to a reduction of the spin disorder scattering and low-temperature formation of a heavy Fermi liquid state. Finally, there is a rapid decrease at T_N, consistent with the further removal of the spin disorder scattering due to magnetic ordering, and a saturation towards a relatively large residual value of $R(T=2K)/R_{300K} = 0.4$.

The magnetic properties were also studied using a PPMS. Results for the magnetic susceptibility $\chi(T)$ and magnetization as a function of magnetic field are shown in Figure 1(*c*,*d*). The $\chi(T)$ data exhibit a Curie-Weiss behavior for $100 K < T < 300$ K, where fits to the data using the expression $\chi(T) = C/(T-\Theta)$ yield an effective (high-temperature) magnetic moment $\mu_{eff} = 3.20\ \mu_B/U$ and $\Theta = -60$ K. That is to be compared with the low temperature AF-ordered magnetic moment of $1.7\ \mu_B/U$ at 4.2 K observed by neutron scattering experiments [36]. The difference between the U moments at high temperature ($3.2\ \mu_B$) and 4.2 K ($1.7\ \mu_B$) indicates the presence of a strong hybridization between the 5*f* electrons of U and '*spd*' conduction electrons, leading to a Kondo-type reduction

of the local U moments. In principle, crystal electric field splitting of the 5*f*-electron multiplet could also result in a reduction of the low temperature moment of U. The AF ordering, where the U magnetic moments are aligned along the *c* axis of the crystal lattice, is seen as a strong decrease in χ(T) below T_N (Fig. 1*c*). The nearly linear response of M(H) at 5 K (Fig. 1*c*), i.e., within the ordered state, is also consistent with antiferromagnetism.

2.2 Synchrotron radiation studies.

Synchrotron high-energy XRD experiments were conducted at the beamline 28-ID-1 at the National Synchrotron Light Source-II, Brookhaven National Laboratory using x-rays with energy of 74.46 keV (λ=0.1665Å). XRD data were collected while varying temperature between 10 K and 400 K in steps of 5 K. Experimental XRD patterns and atomic pair distribution functions (PDFs) derived from the data using standard procedures [37] are summarized in Figure 2.

3. Structure modeling

3.1 Average crystal structure as a function of temperature.

To reveal the evolution of the average crystal structure of UPt_2Si_2 with temperature, synchrotron XRD data were subjected to Rietveld analysis using the software package FullProf [38]. Representative Rietveld fits based on a Space Group (S.G.) *P4/nmm* model are shown in Figures 3(*a*,*b*). The fits were successful and produced the lattice parameters and unit cell volume summarized in Figure 3(*c*,*d*) and Figure 3(*e*), respectively. The *c* lattice parameter and volume are seen to diminish smoothly with decreasing temperature. By contrast, the rate of decrease of the *a* lattice parameter with decreasing temperature changes markedly at T_{CDW}, indicating that the atomic displacements related to the emergent CDW are likely to occur in the basal planes of the crystal lattice.

3.2 Local atomic structure as a function of temperature

As shown in Figure 2(*b*), higher angle Bragg peaks, which are extra sensitive to the local atomic structure, show an intricate evolution with temperature. Inspection of the respective atomic PDFs (Fig. 2(*c*)) which directly reflect frequently occurring atomic pair distances, shows that the peak positioned near 3.0 Å splits into two components below 350 K. The two components increasingly become separated from each other with decreasing temperature and the intensity of the PDF peak at about 4.25 Å suddenly increases below 100 K. The profile of the PDF peak at about 5.5 Å also changes significantly with temperature. The evolution of interatomic distances in UPt_2Si_2 is well illustrated in Fig. 2*d*, where selected atomic PDFs are shown. Here it is seen that, locally, the

crystal lattice continuously evolves with temperature. To assess the evolution in more detail, we fit the experimental PDF data with a model based on the S. G. *P4/nmm* structure using the Rietveld refined structure data as a starting point. Note that atomic PDF analysis is advantageous to Rietveld analysis when exploring local distortions of the crystal lattice because it takes into account both the diffuse and Bragg components of the diffraction data, while Rietveld analysis uses only the latter and, hence, is mainly sensitive to the average long-range crystal structure [39,40].

Fits including interatomic distances within two unit cells of UPt_2Si_2 (up to ~20 Å) are shown in Figure 4. As can be seen in Fig. 4(*a*,*b*), several PDF features, including the sequence of well-defined PDF peaks positioned between 2 Å and 4 Å, and the cluster of overlapping PDF peaks at about 5.5 Å, i.e., the local atomic structure of UPt_2Si_2, are not well reproduced by this model. Therefore, we allowed atoms in the tetragonal unit cell to move away from their position in the undistorted lattice, thus locally breaking the tetragonal lattice symmetry. The fits improved to an acceptable level, demonstrated in Fig. 4(*c*,*d*), only when both Pt(2) and U atoms underwent a considerable displacement from their position in the undistorted lattice, while changes in the position of Pt(1), Si(1) and Si(2) atoms deteriorated the fits. Changes in the position of Pt(2) atoms were expected because prior single crystal studies [29] indicated that they are associated with the CDW in UPt_2Si_2 emerging with decreasing temperature. Changes in the position of U atoms were unexpected.

Fits including interatomic distances longer than 20 Å are shown in Figure 5. As can be seen in Figure 5(*c*,*d*), at 400 K, the lattice distortions in UPt_2Si_2 do not affect its long-range structure significantly. By contrast, at 10 K, the lattice distortions disturb the long-range structure over interatomic distances extending to about 35 Å, above which the average tetragonal crystal symmetry is recovered. Tetragonal lattice parameters and unit cell volume derived from the PDFs in Figure 4 are compared with the Rietveld derived values in Fig. 3(*c*-*e*). A fragment of the PDF-refined crystal structure of UPt_2Si_2 at 10 K and a projection of the fragment on the basal plane (*ab*) of the tetragonal lattice are shown in Figs. 6*a* and Fig. 6*b*, respectively.

4. Discussion

As can be seen in Fig. 3(*c*,*d*), the PDF refined lattice parameters and unit cell volume for UPt_2Si_2 are systematically smaller than the Rietveld refined values. This observation indicates that the local crystal structure is more densely packed in comparison with the bulk values. This may not come as a surprise because the $CaBe_2Ge_2$ structure type is relatively open, allowing the constituent atoms

to change their positions as to minimize the energy of $CaBe_2Ge_2$ structure type compounds when they are subjected to external stimuli. Contrary to the case of Rietveld refined values, the temperature variation of the PDF refined values is uneven, showing inflection points at temperatures close to T_{CDW} and T_N. Moreover, the *a* lattice parameter counterintuitively increases and then barely evolves with temperature over a temperature region centered at T_{coh} (compare data in Fig. 1*b* and Fig. 3*d*). Evidently, changes in the transport and magnetic properties of UPt_2Si_2 and those in its local atomic structure are strongly correlated.

Among all atoms in the unit cell, only the Pt(2) atoms in the Si(2)-Pt(2)-Si(2) planes and the U atoms positioned between the planes (see Fig. 6*a*) are significantly displaced from their positions in the undistorted lattice. For both atoms, the in-plane component of the displacement is much larger than the out-of-plane component. Also, the in-plane component of the displacements for Pt(2) atoms is larger than the in-plane component of U displacements. The opposite is true for the out-of-plane components. In particular, the in-plane displacement for Pt(2) atoms increases with diminishing temperature from a value of 0.04 Å at 400 K to a value of 0.15 Å at 10 K. By contrast, the Pt(2) out-of-plane displacement decreases from the 400 K value of 0.014 Å to the near negligeable value of 0.004 Å at 10 K. On the other hand, the in-plane displacement for U atoms decreases with decreasing temperature from a value of 0.07 Å at 400 K to a value of 0.03 Å at 10 K. At the same time, the out-plane displacement for U atoms barely increases from its 400 K value of about 0.005 Å to 0.009 Å at 10 K. Notably the displacements for Pt(2) and that for U atoms concurrently evolve with diminishing temperature, clearly indicating the presence of significant *5d-5f* electron hybridization in UPt_2Si_2. Overall, the displacements of Pt(2) and U atoms follow a repetitive pattern, characteristic to PLDs known to accompany CDWs. In line with recent single crystal studies [29], the PLDs are largely confined to the basal layers comprising Pt(2) atoms sandwiched between Si planes. However, because both Pt(2) and U atoms are also considerably displaced in an out-of-plane direction, the CDW appearing in UPt_2Si_2 below 315 K is essentially a 3D modulation of the crystal lattice. Signatures of the CDW transition are seen as a sudden increase in the resistivity (Figure 1*b*) and wedge-like bump in the specific heat appearing between 305 K and 320 K [29, 41].

From the structure data obtained in this and previous studies [29], the following picture for the relationship between lattice, electronic and magnetic degrees of freedom in UPt_2Si_2 emerges. At temperatures well above T_{CDW}, Pt(2) and U atoms are already displaced from their positions in the

undistorted tetragonal lattice. The displacements may be viewed at as a precursor of the PLDs emerging below T_{CDW} [29]. Likely because the PLDs are short ranged near T_{CDW}, i.e., do not disturb long-range structure (> 20 Å) of UPt_2Si_2 significantly (see Fig. 5*b,d*), the emerged CDW appears commensurate with the underlying tetragonal crystal lattice. Nonetheless, the PLDs are large enough to increase the local atomic packing significantly in comparison to the average structure. The nonuniform change in the atomic displacements, related bonding distances and local volume with temperature may be expected to render the thermal evolution of transport and magnetic properties nonlinear because the volume and electronic structure of heavy fermion liquids from the $CaBe_2Ge_2$-type family are strongly coupled [42]. In particular, the slow increase in the electrical resistivity upon decreasing temperature below T_{CDW} can be associated with the gradual increase in the in-plane Pt(2) and out-of-plane U displacements, the latter of which reaches a plateau at $T_{coh.}$. The in-plane displacements of uranium, U_{ab}, also reach a plateau at T_{coh} (see Fig. 6*c*). The subsequent decrease in the resistivity with decreasing temperature mirrors the decrease in the out-of-plane Pt(2) displacements. Then, the high value of the residual resistivity at very low temperatures can be attributed to residual electron-phonon scattering arising from the significant in-plane Pt(2) and out-of-plane U displacements. In addition, the local breaking of crystal symmetry will affect the crystal field splitting of the U *5f*-elecron multiplet and, hence, contribute to the observed changes in the magnetic moment of U atoms with temperature. Moreover, the periodic displacement of U atoms and related periodic modulation of the local crystal symmetry may modulate the AF ordered pattern of U magnetic moments below T_N, as observed by resonant x-ray scattering experiments [43]. The observed irreversibility in the magnetic susceptibility below T_N can also be explained by the presence of local lattice distortions involving the magnetically active U atoms [44]. Finally, the coupled sharp increase and decrease of Pt and U atomic displacements below T_N signals an increased lattice instability, which may contribute to the complex magnetic phase diagram observed below 20 K in high magnetic fields [34]. The increased lattice instability is also demonstrated by the increased spatial extent of the PLDs distortions (~ 35 Å) at low temperatures (Fig. 5*a,c*). The latter can be a major factor behind the observed [29] change of the character of the CDW from initially commensurate at high temperature to distinctly incommensurate at low temperature. More precisely, it could be that, at low temperature, the incommensurate CDW structure of UPt_2Si_2 consists of commensurate CDW domains with a size of about 35 Å, separated by discommensurations, e.g., narrow domain walls where the CDW phase

changes fast [45]. Analysis of single crystal experiments suggests that the observed satellites signaling the emerged CDW order can indeed be regarded as overlapped patterns arising from such domains [29].

Conclusion

Magnetic, transport and bonding phenomena in heavy fermion liquids such as UPt_2Si_2 are sensitive to the degree of hybridization between localized U 5*f* orbitals and (*spd*) conduction electrons, which, in turn, depends on the interatomic distances and crystal lattice symmetry. The spatial extent of the orbitals and their proximity to the Fermi level render these materials susceptible to external stimuli and give rise to competing crystallographic modifications, including local variations in the atomic positions, packing density and volume. As our study shows, the variations in the atomic positions largely involve in-plane Pt and out-of-plane U displacement modes, thus forming an exotic 3D CDW below T_{CDW}. In addition, they progress nonlinearly with decreasing temperature, inevitably leading to concurrent non-linear changes in both the magnetic and transport properties. The results suggest that the marked flexibility of the crystal lattice must be accounted for in order to understand the rich physics of UPt_2Si_2 and, by extension, other heavy 5*f* fermion liquids in general.

Acknowledgements

This work was supported by the U.S. Department of Energy, Office of Science, Office of Basic Energy Sciences under Award No. DE-SC0021973 and used resources of the National Synchrotron Light Source at the Brookhaven National Laboratory provided by the DOE Office of Science under Contract No DE-SC0012704. Thanks are due to Dr. D. R. Tadisetti for the help with Rietveld analysis. RB was supported by the National Science Foundation through NSF DMR-1904361. The National High Magnetic Field Laboratory is supported by the National Science Foundation through NSF DMR-1644779 and the State of Florida.

References:

1. I. Osborne and R. Coontz, Quantum wonderland *Science* **319**, 1201 (2008).
2. Q. Si and F. Steglich, Heavy fermions and quantum phase transitions Science **329**, 1161 (2010).
3. P. Monthoux, D. Pines, and G. G. Lonzarich Superconductivity without phonons Nature **450**, 1177 (2007).
4. C. Broholm, R. J. Cava, S. A. Kivelson, D. G. Nocera, M. R. Norman, T. Senthil Science 6475, **367** (2020).
5. V. Martelli, A. Cai, E. M. Nica, S. Paschen Sequential localization of a complex electron fluid *PNAS* **116**, 17701 (2019).
6. J.A. Mydosh, P.M. Oppeneer and P.S. Riseborough, Hidden order and beyond: an experimental—theoretical overview of the multifaceted behavior of URu_2Si_2 J. Phys.: Condens. Matter **32**, 143002 (2020).
7. A.D. Huxley, Ferromagnetic superconductors Physica C **514**, 368 (2015).
8. See for example the Proceedings of the Strongly Correlated Electron System Conference, Amsterdam 24 – 29 July 2022; https://scipost.org/SciPostPhysProc.202205001
9. M. Shatruk, $ThCr_2Si_2$ structure type: The "perovskite" of intermetallics J. Solid State Chem. **272**, 198 (2019).
10. Y. Lai, J. Y. Chan, and R. E. Baumbach, Electronic landscape of the f-electron intermetallics with the $ThCr_2Si_2$ structure Sci. Adv. **8**, eabp8264 (2022).
11. Y. Lai, K. Wei, G. Chappell, J. Diaz, T. Siegrist, P. J. W. Moll, D. Graf, R. E. Baumbach, Tuning the structural and antiferromagnetic phase transitions in UCr_2Si_2: Hydrostatic pressure and chemical substitution Phys. Rev. Mater. **4**, 075003 (2020).
12. H. Q. Yuan, F. M. Grosche, M. Deppe, C. Geibel, G. Sparn, F. Steglich, Observation of two distinct superconducting phases in $CeCu_2Si_2$ Science **302**, 2104 (2003)
13. E. Schuberth, M. Tippmann, L. Steinke, S. Lausberg, A. Steppke, M. Brando, C. Krellner, C. Geibel, R. Yu, Q. Si, F. Steglich, Emergence of superconductivity in the canonical heavy-electron metal $YbRh_2Si_2$ Science **351**, 485 (2016).
14. H. S. Jeevan, C. Geibel, Z. Hossain, Quasiquartet crystal-electric-field ground state with possible quadrupolar ordering in the tetragonal compound $YbRu_2Ge_2$ Phys. Rev. B **73**, 020407 (2006).
15. Z. Ren, L. V. Pourovskii, G. Giriat, G. Lapertot, A. Georges, D. Jaccard, Giant overlap between the magnetic and superconducting phases of $CeAu_2Si_2$ under pressure Phys. Rev. X **4**, 031055 (2014).
16. S. Süllow, M. C. Aronson, B. D. Rainford, P. Haen, Doniach phase diagram, revisited: From ferromagnet to Fermi liquid in pressurized $CeRu_2Ge_2$ Phys. Rev. Lett. **82**, 2963 (1999).
17. M. B. Fontes, M. A. Continentino, S. L. Bud'ko, M. El-Massalami, L. C. Sampaio, A. P. Guimarães, E. Baggio-Saitovitch, M. F. Hundley, A. Lacerda, Physical properties of the Ce $(Ru_{1-x}\,Fe_{x)2}Ge_2$ series Phys. Rev. B **53**, 11678 (1996).
18. L. C. Gupta, D. E. MacLaughlin, C. Tien, C. Godart, M. A. Edwards, R. D. Parks, Magnetic behavior of the Kondo-lattice system $CeRu_2Si_2$ Phys. Rev. B **28**, 3673 (1983).
19. K. Hiebl, C. Horvath, P. Rogl, Magnetic behaviour of ternary silicides CeT_2Si_2 (T= Ru, Rh, Pd, OS, Ir, Pt) and boron substitution in $Ce\{Ru, Os\}_2\,Si_{2-x}B_2$ J. Less Common Met. **117**, 375 (1986).
20. M. Mihalik, M. Mihalik V. Sechovsky, Electrical transport and magnetism in $CeFe_2Si_2$ single crystal Physica B **359**, 163 (2005).
21. H. Abe, K. Yoshii, H. Kitazawa, Complex magnetic phase diagram of $CeRu_2Ge_2$ Physica B

312, 253 (2002).
22. H. H. Lai, S. E. Grefe, S. Paschen and Q. Si, Weyl–Kondo semimetal in heavy-fermion systems PNAS **115**, 93 (2017).
23. S. Süllow, G. J. Nieuwenhuys, A. A. Menovsky, J. A. Mydosh, S. A. M. Mentink, T. E. Mason, W. J. L. Buyers, Spin glass behavior in URh_2Ge_2 Phys. Rev. Lett. **78,** 354 (1997).
24. H. Ptasiewicz-Bak, Neutron diffraction study of magnetic ordering in UPd_2Si_2, UPd_2Ge_2, URh_2Si_2 and URh_2Ge_2 J. Phys. F Met. Phys. **11**, 1225 (1981).
25. M. Kuznietz, H. Pinto, H. Ettedgui, M. Melamud, Neutron-diffraction study of the magnetic structure of UCo_2Ge_2 Phys. Rev. B **40**, 7328 (1989).
26. T. Endstra, G. J. Nieuwenhuys, A. A. Menovsky, J. A. Mydosh, Structural and magnetic properties of UCo_2Ge_2 J. Appl. Phys. **69**, 4816 (1991).
27. A. Gallagher, K. W. Chen, C. M. Moir, S. K. Cary, F. Kametani, N. Kikugawa, D. Graf, T. E. Albrecht-Schmitt, S. C. Riggs, A. Shekhter, R. E. Baumbach, Unfolding the physics of URu_2Si_2 through silicon to phosphorus substitution Nat. Commun. **7**, 10712 (2016).
28. Y. Dalichaouch, M. B. Maple, J. W. Chen, T. Kohara, C. Rossel, M. S. Torikachvili, A. L. Giorgi, Effect of transition-metal substitutions on competing electronic transitions in the heavy-electron compound URu_2Si_2 Phys. Rev. B **41**, 1829 (1990).
29. J. Lee, K. Prokes, S. Park, I. Zaliznyak, S. Dissanayake, M. Matsuda, M. Frontzek, S. Stoupin, G. L. Chappell, R. E. Baumbach, C. Park, J. A. Mydosh, G. E. Granroth, J. P. C. Ruff, Charge density wave with anomalous temperature dependence in UPt_2Si_2 Phys. Rev. B **102**, 041112 (2020).
30. G. J. Nieuwenhuys, Crystalline electric field effects in UPt_2Si_2 and URu_2Si_2 Phys. Rev. B **35**, 5260 (1987).
31. D. S. Grachtrup, M. Bleckmann, B. Willenberg, S. Süllow, M. Bartkowiak, Y. Skourski, H. Rakoto, I. Sheikin, and J. A. Mydosh, Field-induced phases in UPt_2Si_2 Phys. Rev. B **85**, 054410 (2012).
32. S. Elgazzar, J. Rusz, P. M. Oppeneer, and J. A. Mydosh, Electronic structure and Fermi surface of paramagnetic and antiferromagnetic UPt_2Si_2 Phys. Rev. B **86**, 075104 (2012).
33. D. S. Grachtrup, N. Steinki, S. Süllow, Z. Cakir, G. Zwicknagl, Y. Krupko, I. Sheikin, M. Jaime, and J. A. Mydosh, Magnetic phase diagram and electronic structure of UPt_2Si_2 at high magnetic fields: A possible field-induced Lifshitz transition Phys. Rev. B **95**, 134422 (2017).
34. J. Lee, M. Matsuda, J. A. Mydosh, I. Zaliznyak, A. I. Kolesnikov, S. Süllow, J. P. C. Ruff, and G. E. Granroth, Dual nature of magnetism in a uranium heavy-fermion system Phys. Rev. Lett. **121**, 057201 (2018)
35. S. Süllow, A. Otop, A. Loose, J. Klenke, O. Prokhnenko, R. Feyerherm, R. W. A. Hendrikx, J. A. Mydosh, and H. Amitsuka, J. Phys. Soc. Jpn. **77**, 024708 (2008).
36. R. A. Steeman, E. Frikkee, S. A. M. Mentink, A. A. Menovsky, G. J. Nieuwenhuys and J. A. Mydosh, Hybridisation effects in UPt_2Si_2 J. Phys.: Condens. Matter **2,** 4059 (1990).
37. C. L. Farrow, P. Juhás, J. W. Liu, D. Bryndin, E. S. Božin, J. Bloch, Th. Proffen, and S. J. L. Billinge, PDFfit2 and PDFgui: computer programs for studying nanostructure in crystals J. Phys.: Condens. Matter **19**, 335219 (2007).
38. J. Rodriguez-Carvajal, FullProf for magnetic structures. New features Physica B **192**, 55 (1993).
39. T. Egami and S.J.L. Billinge in "Underneath the Bragg peaks: structural analysis of complex materials" *(Elsevier, 2003).*

40. V. Petkov Pair distribution functions analysis, *Willey's Characterization of Materials* (2012).
41. M. Bleckmann, A. Otop, S. Sullow, R. Feyerherm, J. Klenke, A. Loose, R. W. A. Hendrikx, J. A. Mydosh, and H. Amitsuka, Structural properties, magnetic order and electronic transport in single crystalline UPt_2Si_2 J. Magn. Magn. Mater. **322**, 2447 (2010).
42. Y. Lai, J. Y. Chan, and R. E. Baumbach, Electronic landscape of the f-electron intermetallics with the $ThCr_2Si_2$ structure *Sci. Adv.* **8**, eabp8264 (2022).
43. F. Kon, C. Tabata, K. Miura, R. Hibino, H. Hidaka, T. Yanagisawa, H. Nakao and A. Amitsuka, Correlation between Antiferromagnetic and Charge-Density-Wave Order in UPt_2Si_2 Studied by Resonant X-Ray Scattering SciPost Physics (2023) https://scipost.org/preprints/scipost_202208_00025v1/
44. A. Otop, F. J. Litterst, R. W. A. Hendrikx, J. A. Mydosh and S. Sullow, Magnetic irreversibility in single crystalline UPt_2Si_2 J. Appl. Phys. **95**, 6702 (2004).
45. H. J. Kim, C. D. Malliakas, A. T. Tomic, S. H. Tessmer, M. G. Kanatzidis, and S. J. L. Billinge, Local atomic structure and discommensurations in the charge density wave of $CeTe_3$ Phys. Rev. Lett. **96**, 226401 (2006).

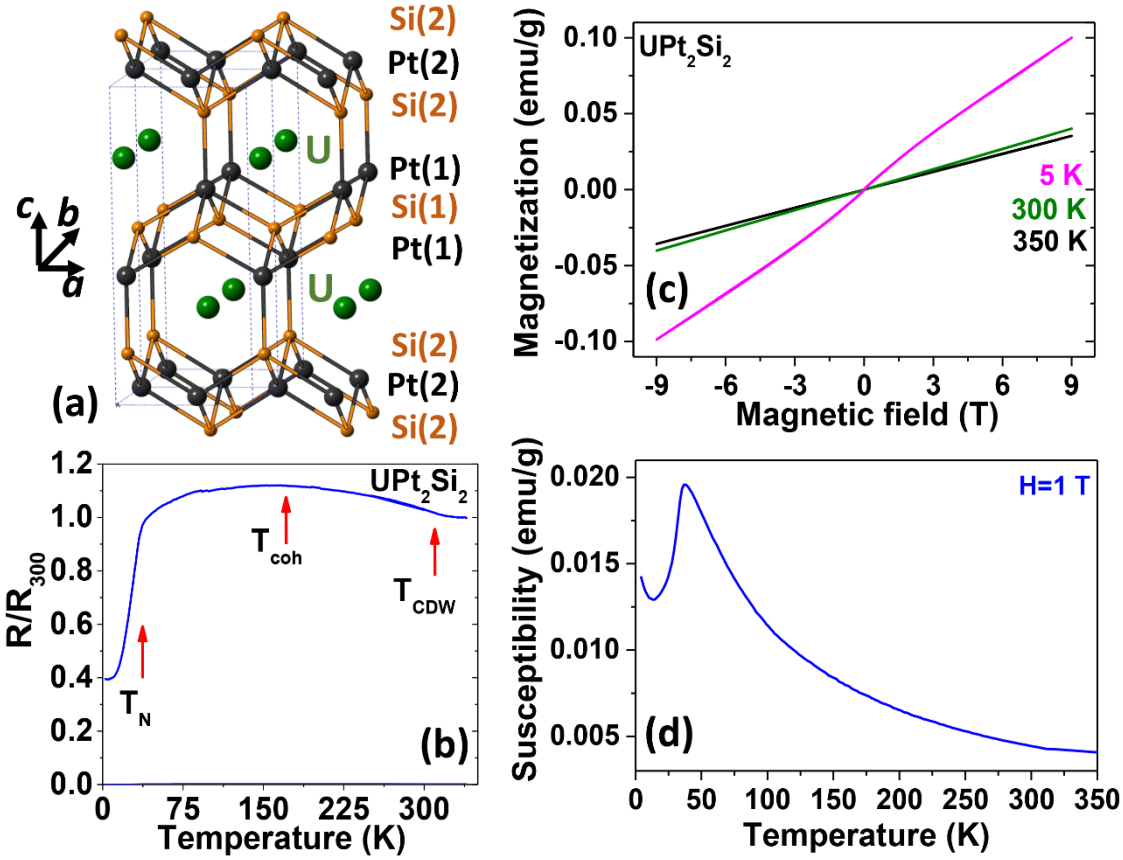

Figure 1. (***a***) Fragment from the crystal structure of UPt_2Si_2 featuring a sequence of alternating Pt(1)-Si(1)-Pt(1) and Si(2)-Pt(2)-Si(2) layers and uranium U atoms (in green) positioned between the layers. Pt atoms are in black and Si atoms are in brown. (***b***) Resistivity of UPt_2Si_2 as a function of temperature. Arrows mark inflection points on the resistivity vs temperature curve corresponding to the onset of a charge density wave (T_{CDW}), change of conductivity type (T_{coh}) and emergence of antiferromagnetic (T_N) order. (***c***) Hysteresis curves (magnetization vs external magnetic field) for UPt_2Si_2 measured at three different temperatures. (***d***) Magnetic susceptibility $\chi(T)$ for UPt_2Si_2. The broad peak at T_N=37 K reflects the emergence of an antiferromagnetic order with decreasing temperature.

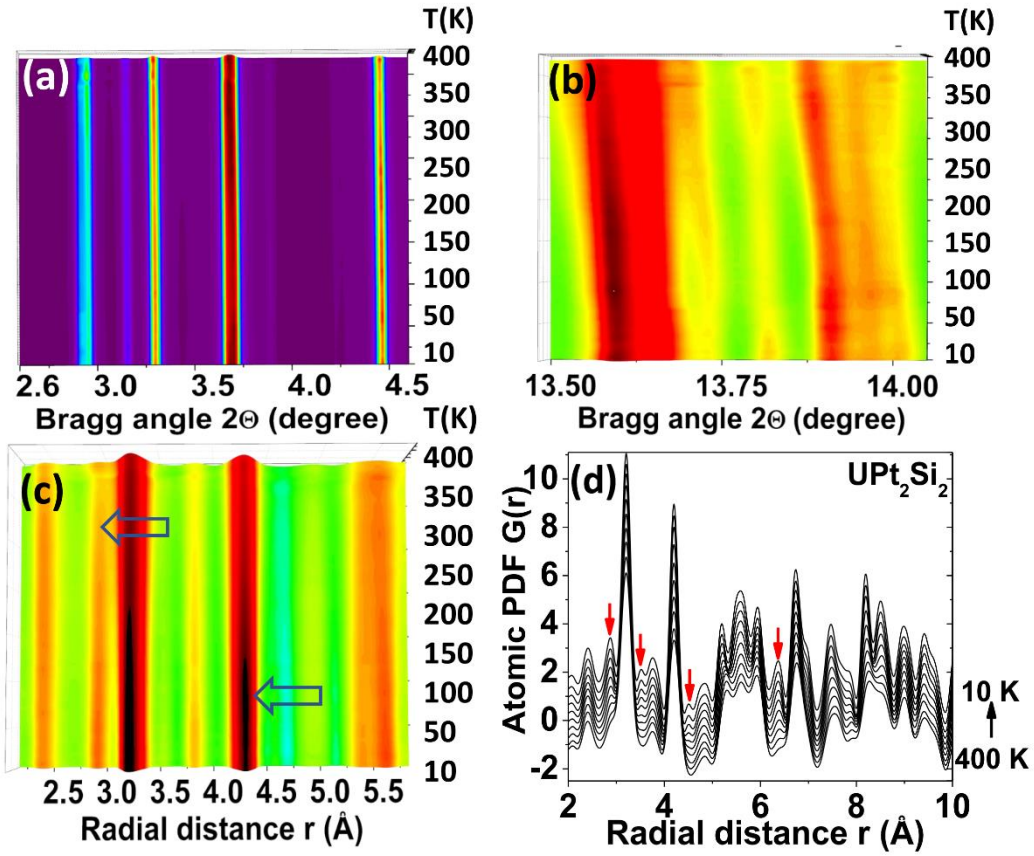

Figure 2. (***a, b***) XRD intensity color maps for UPt_2Si_2 collected in the temperature range from 10 K to 400 K. The maps cover different ranges of Bragg angles. While the low angle Bragg peaks do not those at higher angles show a complex evolution with temperature. (***c***) Atomic PDF intensity color map for UPt_2Si_2. The PDF peak at about 3 Å splits into two components below T_{CDW} = 315 K. The intensity of the peak at 4.25 Å suddenly starts increasing below 100 K (see the horizontal arrows). (***d***) Selected atomic PDFs for UPt_2Si_2. Vertical arrows mark PDF features, i.e., atomic pair distances, that evolve markedly with temperature.

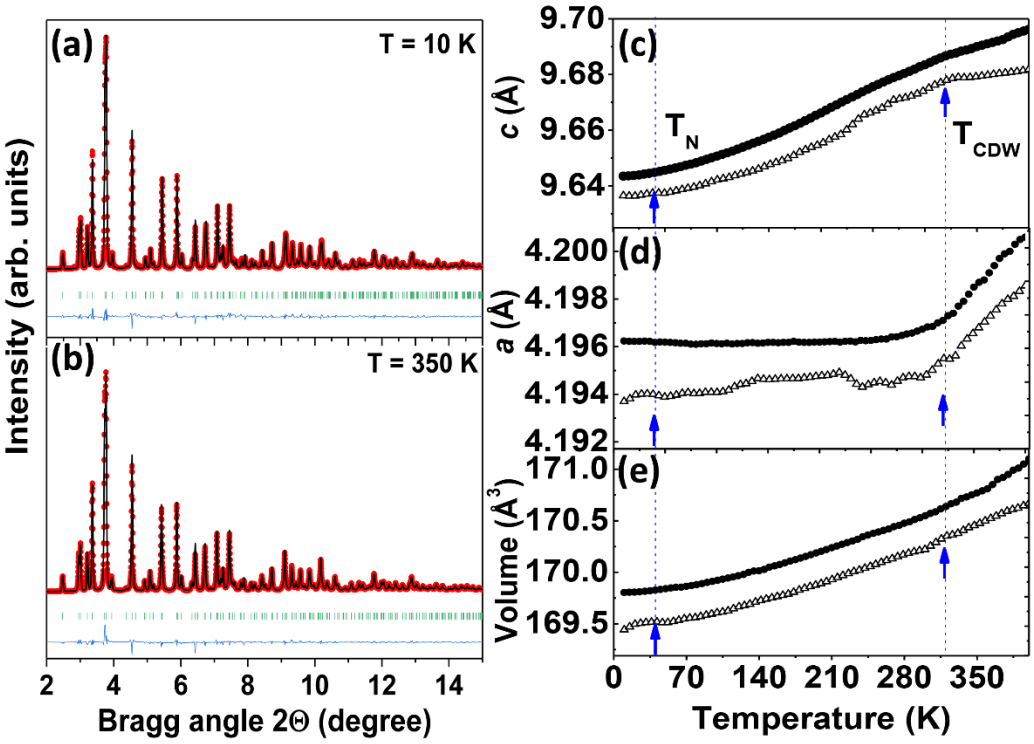

Figure 3. (***a, b***) Successful Rietveld fits to XRD patterns for UPt_2Si_2. The fits are based on a tetragonal (S.G. *P4/nmm*) model as explained in the text. The goodness-of-fit factor R_{wp} for the fits are in the order of 9 %. Experimental data are given as symbols, the computed data are given as red lines and the residual difference (shifted for clarity) is given as a blue line. (***c,d,e***) Rietveld refined tetragonal lattice parameters and unit cell volume given as solid symbols. PDF refined lattice parameters and unit cell volume are also given as open symbols. Blue arrows mark inflection points on the lattice parameters vs temperature curves where CDW (T_{CDW}) and AF (T_N) orders emerge on cooling. The difference between Rietveld and PDF values indicates that, locally, the atomic arrangement in UPt_2Si_2 is more compressed in comparison to the average crystal structure. Error bars in (c,d,e) are close to the size of used symbols.

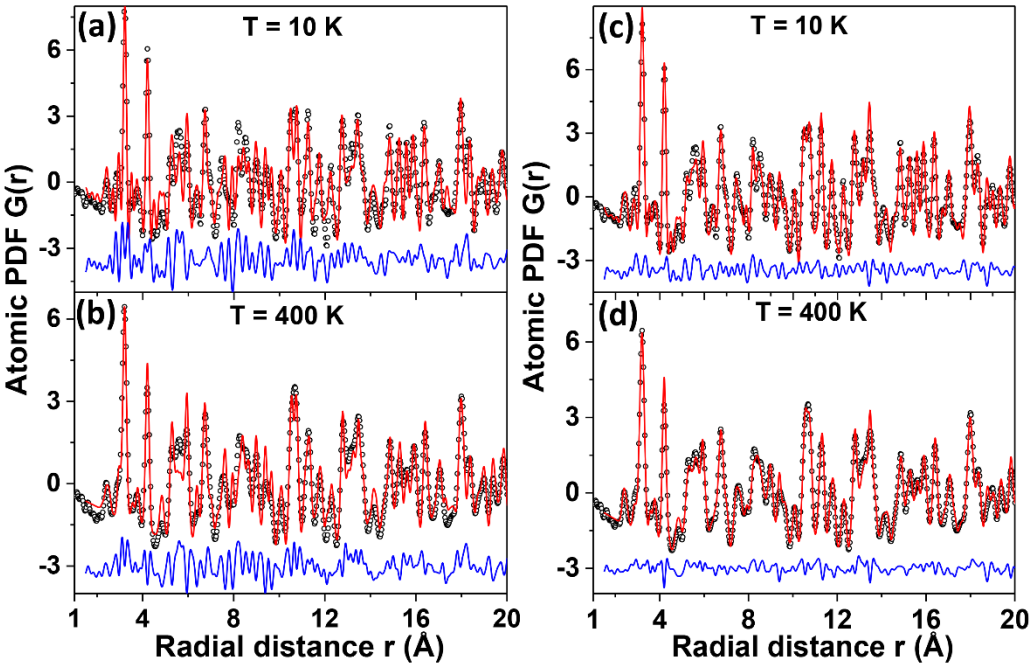

Figure 4. (***a, b***) Unsuccessful and (***c,d***) successful fits to the low-r part of PDFs for UPt_2Si_2 obtained at two characteristic temperatures. The unsuccessful fits are based on a tetragonal (S.G. *P4/nmm*) model while the successful fits are based on a tetragonal (S.G. *P4/nmm*) model where the local symmetry is broken as explained in the text. The goodness-of-fit factor R_{wp} for the unsuccessful fits is in the order of 40 % while that for the successful fits is in the order of 12 %. Experimental data are given as symbols, computed data are given as red lines and the residual difference (shifted for clarity) is given as a blue line.

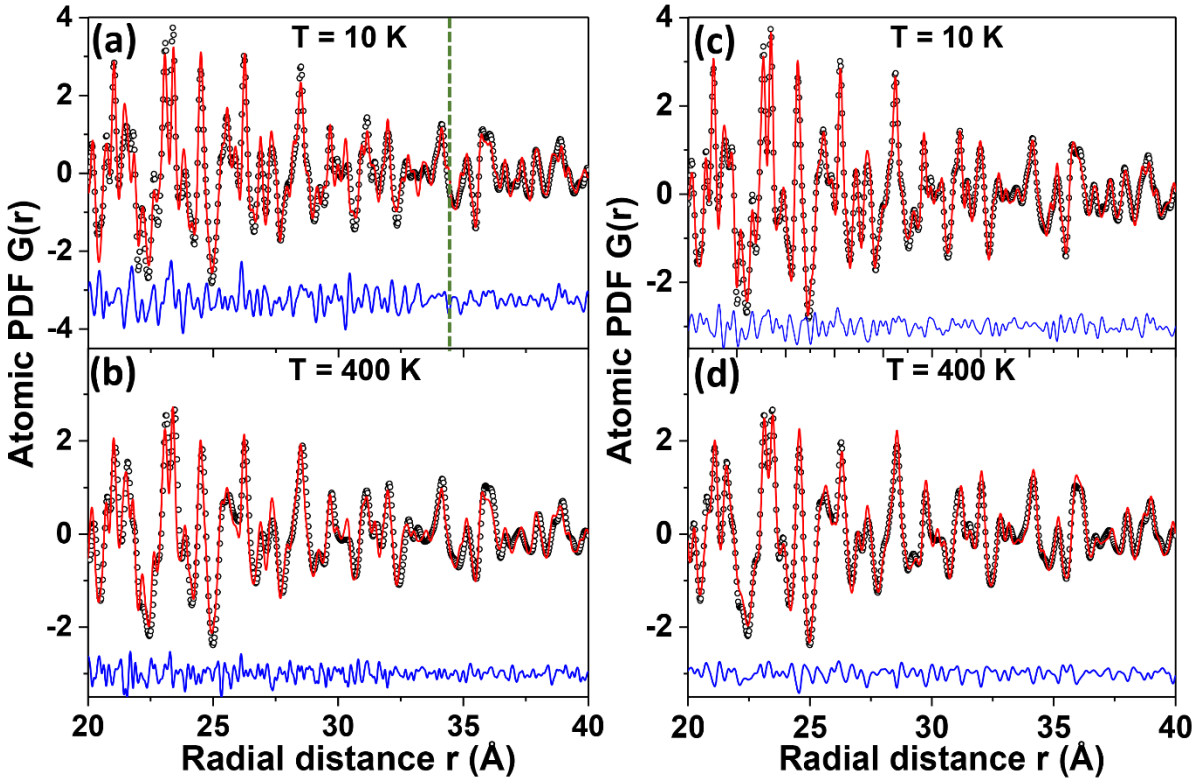

Figure 5. (***a***) Unsuccessful and (***c***) successful fit to the higher-r part of the PDF for UPt_2Si_2 obtained at 10 K. The unsuccessful fit is based on a tetragonal (S.G. *P4/nmm*) model while the successful fit is based on a tetragonal (S.G. *P4/nmm*) model where the local symmetry is broken as explained in the text. The latter model also fits well the low-r part of the 10 K PDF data set, as shown in Fig. 4(***c***). (***b,d***) Near equally successful fits to the high-r part of the PDF for UPt_2Si_2 obtained at 400 K. The fits are based on (***b***) an unmodified tetragonal (S.G. *P4/nmm)* model and (***d***) a tetragonal (S.G. *P4/nmm*) model where the local symmetry is broken as explained in the text. Evidently, at high temperature, the lattice distortions in UPt_2Si_2 leave its long-range structure largely intact, i.e., they needn't be necessarily evoked to explain it, which is not true for the shorter-range structure (see Fig. 4***b***). By contrast, at low temperature, the lattice distortions significantly disturb the long-range structure of UPt_2Si_2 up to distances of about 35 Å (vertical broken line in (***a***)), above which the average tetragonal crystal symmetry is recovered (see the sharp drop in the fit residual). The goodness-of-fit factor R_{wp} for the unsuccessful fit in (***a***) is 28 % while that for the successful fits is in the order of 12 %. Experimental data are given as symbols, computed data are given as red lines and the residual difference (shifted for clarity) is given as a blue line.

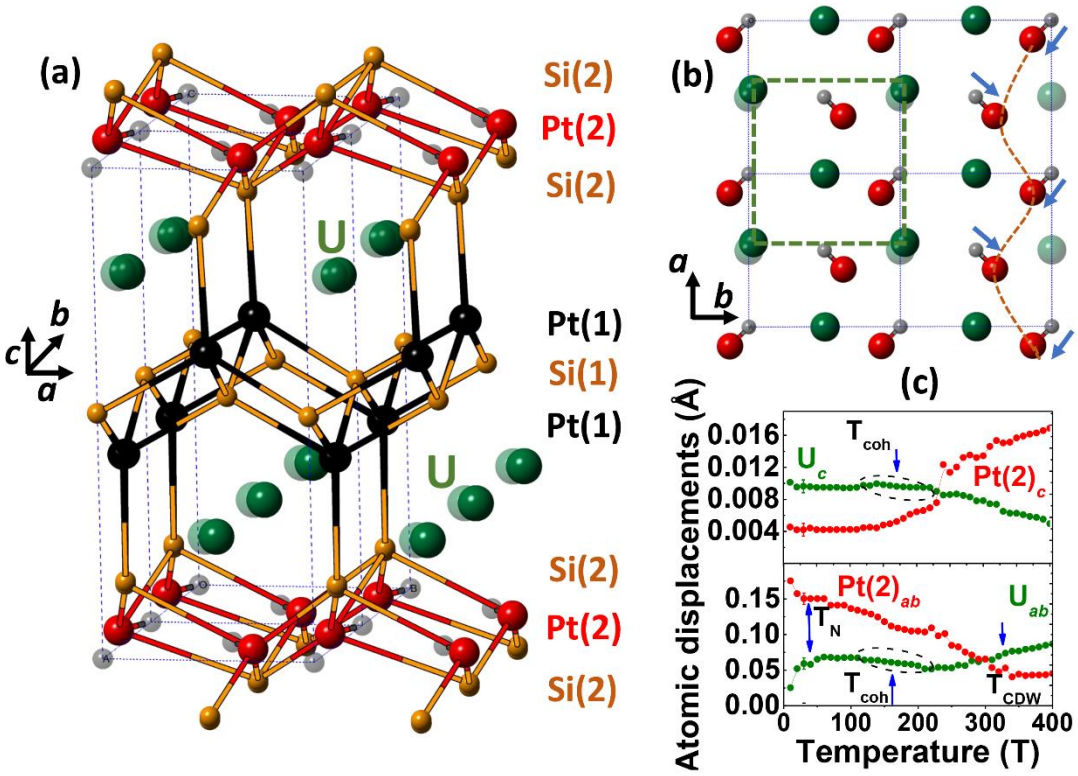

Figure 6. (***a***) Fragment from the structure of UPt_2Si_2 at 10 K as derived from PDF analysis where Pt(2) atoms (red circles) appear displaced from their positions in the undistorted tetragonal structure (light gray circles). Uranium atoms (solid green circles) also appear displaced from their positions in the undistorted lattice (light green circles). By contrast, Si(1), Si(2) and Pt(1) are not displaced significantly from their positions in the undistorted lattice. (***b***) Projection of the displacements of Pt(2) and U atoms on the (*ab*) atomic plane. Blue arrows point in the direction of Pt(2) displacements. Brown broken line, resembling a sine wave, emphasizes the periodicity in the Pt(2) atom displacements, forming a PLD. The same pertains to the green broken line connecting the positions of displaced U atoms. (***c***) Amplitude of the atomic displacements of Pt(2) and U atoms from their positions in the undistorted lattice. Blue arrows mark inflection points on the displacement's vs temperature curves where the CDW (T_{CDW}) and AF (T_N) orders set it. Black broken lines highlight a range of temperatures, centered at about $T_{coh.}$ = 150 K, where, counterintuitively, the vertical and in-plane displacements of U atoms increase with diminishing temperature before reaching 100 K, and then remain unchanged down to 10 K. Error bars in (***c***) are close to the size of used symbols.